Multi-Window Post-Doppler Dimensionality Reduction for Multi-Waveform STAP

Lumumba Harnett[1], Patrick M. McCormick[1], Shannon D. Blunt[1], Justin G. Metcalf[2]
[1]Radar Systems Lab, University of Kansas, Lawrence, KS
[2]Sensors Directorate, Air Force Research Laboratory, Dayton, OH

***Abstract* – A multi-waveform version of space-time adaptive processing, denoted as MuW-STAP (or μ-STAP), was recently developed as a single-input multiple-output (SIMO) emission scheme that incorporates training data generated by multiple secondary filters into the estimation of the sample covariance matrix. This integration of additional training data was found to increase robustness to non-homogeneous clutter because the secondary filters serve to "homogenize" the interference in range. Here we incorporate μ-STAP into multi-window post-Doppler STAP (specifically PRI-Staggered and Adjacent-Bin implementations) to assess the impact when dimensionality reduction techniques are employed. SINR analysis was used to evaluate the performance of these reduced dimension μ-STAP formulations under various simulated clutter conditions.**

***Keywords*– GMTI, STAP, SIMO radar**

I. INTRODUCTION

In [1-3] a multi-waveform version of space-time adaptive processing (STAP) denoted as μ-STAP was proposed for ground moving target indication (GMTI) from an airborne platform. The purpose of STAP in general is to provide clutter (and other interference) cancellation through estimation of the covariance matrix in a given cell-under-test (CUT) for subsequent determination of whether a moving target is present [4,5]. However, due to non-homogeneity effects such as clutter non-stationary, internal clutter motion, and contamination of training data by targets of interest, precise estimation of the clutter covariance matrix remains a difficult problem [6-9]. In addition, STAP has practical constraints due to the computational complexity involved with repeatedly estimating and inverting a sample covariance matrix and the requirements on representative sample support [4].

The μ-STAP approach was developed [1-3] to address non-homogeneity effects through the use of secondary pulse compression filters that serve to homogenize the range domain response. Both single-input multiple-output (SIMO) and multiple-input multiple-output (MIMO) instantiations of μ-STAP have been examined [1-3], with the latter also transmitting the waveforms corresponding to the secondary receive filters. Because it does not require modification to an existing airborne radar system, here we consider the SIMO formulation of μ-STAP and assess the impact of incorporating well-known reduced-dimension STAP implementations.

II. MULTI-WAVEFORM STAP

The SIMO version of μ-STAP relies on the traditional STAP emission structure of a single waveform, here denoted as the "primary" waveform $s_{\text{prime}}(t)$, in a given spatial direction via array beamforming. Thus the received response from the illuminated scattering and noise for the mth pulse of M in the coherent processing interval (CPI) at the nth antenna element of N can be modelled as [3]

$$y(m,n,t) = \sum\sum \Big[s_{\text{prime}}(t) * x_{\text{prime}}(t,\theta,\omega,\theta_{\text{look}}) \Big] e^{j(m\omega+n\theta)} + v_{\text{noise}}(t) + v_{\text{jam}}(t) \quad , \quad (1)$$

where $x_{\text{prime}}(t,\theta,\omega,\theta_{\text{look}})$ is the collection of scattering induced by the primary waveform as a function of Doppler ω, spatial angle θ, and the transmit beampattern, with $v_{\text{noise}}(t)$ additive noise and $v_{\text{jam}}(t)$ barrage jamming. Per [1-3], the μ-STAP formulation performs pulse compression filtering using $h_{\text{prime}}(t)$, that is the matched/mismatched filter for the primary waveform, as well as with the set of K secondary filters denoted $h_{\text{sec},1}(t), h_{\text{sec},2}(t), \ldots, h_{\text{sec},K}(t)$ as

$$\begin{aligned} z_{\text{prime}}(m,n,t) &= h_{\text{prime}}(t) * y(m,n,t) \\ z_{\text{sec},1}(m,n,t) &= h_{\text{sec},1}(t) * y(m,n,t) \\ z_{\text{sec},2}(m,n,t) &= h_{\text{sec},2}(t) * y(m,n,t) \\ &\vdots \\ z_{\text{sec},K}(m,n,t) &= h_{\text{sec},K}(t) * y(m,n,t) \end{aligned} \quad . \quad (2)$$

The secondary filters produce a smearing in range, with a different (low) cross-correlation sidelobe structure for each primary waveform / secondary filter pair. The result is a mixing in range of the ubiquitous clutter, smeared de-emphasis of targets in the training data, and smeared capture in the training data of large discretes that may reside in the CUT. Discretizing the filter outputs of (2) in the range domain and collecting the MN samples of each for range index ℓ yields the $K+1$ space-time snapshots $\mathbf{z}_{\text{prime}}(\ell)$ and $\mathbf{z}_{\text{sec},k}(\ell)$ for $k = 1, 2, \ldots, K$. Defining $\mathbf{c}_{\text{s}}(\theta_{\text{prime}})$ as the spatial steering vector for look direction θ_{prime} and $\mathbf{c}_{\text{t}}(\omega_{\text{D}})$ as the temporal steering vector for Doppler frequency ω_{D}, the combined space-time steering vector is

$$\mathbf{c}_{\text{st}}(\theta_{\text{prime}}, \omega_{\text{D}}) = \mathbf{c}_{\text{t}}(\omega_{\text{D}}) \otimes \mathbf{c}_{\text{s}}(\theta_{\text{prime}}) \, , \quad (3)$$

where $\otimes$ is the Kronecker product. For the space-time covariance matrix $\mathbf{R}(\ell_{\text{CUT}})$ corresponding to the CUT, the STAP filter is [4,5]

This work was supported in part by a subcontract with Matrix Research, Inc. for research sponsored by AFRL under Prime Contract No. FA8650-14-D-1722, by the NSF Graduate Research Fellowship Program under Grant No. DGE-1451148, and by the University of Kansas Chancellor's Fellowship.

$$\mathbf{w}(\ell_{\text{CUT}},\theta_{\text{prime}},\omega_{\text{D}})=\mathbf{R}^{-1}(\ell_{\text{CUT}})\mathbf{c}_{\text{st}}(\theta_{\text{prime}},\omega_{\text{D}})\,, \qquad (4)$$

for application to the CUT snapshot as

$$\alpha(\ell_{\text{CUT}},\omega_{\text{D}})=\mathbf{w}^{H}(\ell_{\text{CUT}},\theta_{\text{look}},\omega_{\text{D}})\mathbf{z}_{\text{prime}}(\ell_{\text{CUT}})\,, \qquad (5)$$

followed by comparison with a detection threshold.

The well-known sample covariance matrix (SCM) estimate is

$$\hat{\mathbf{R}}_{\text{prime}}(\ell_{\text{CUT}})=\frac{1}{n(L_{\text{prime}})}\sum_{\substack{\ell\in L_{\text{prime}}\\ \ell\neq\ell_{\text{CUT}}}}\mathbf{z}_{\text{prime}}(\ell)\mathbf{z}_{\text{prime}}^{H}(\ell)\,, \qquad (6)$$

for $n(L_{\text{prime}})$ the cardinality of the set L_{prime} of primary snapshots, with ℓ_{CUT} excluded to avoid self-cancellation. The SCM is often diagonally loaded to ensure full rank by adding $\sigma_v^2\mathbf{I}_{MN}$ to (6), for σ_v^2 the noise power and $\mathbf{I}_{MN}$ an $MN\times MN$ identity matrix. In [1-3] a new SCM matrix was proposed that instead relies on the space-time snapshots obtained from the secondary filtering in (2) based on the logic that, since the SCM formulation aggregates the interference across range snapshots anyway, a mixing in range beforehand preserves this property while also smoothing out the non-stationary effects. The "no primary" (NP) version of the μ-STAP SCM is

$$\hat{\mathbf{R}}_{\mu,\text{NP}}(\ell_{\text{CUT}})=\frac{1}{n(L_{\text{sec}})K}\sum_{i=1}^{K}\sum_{\ell\in L_{\text{sec}}}\mathbf{z}_{\text{sec},i}(\ell)\mathbf{z}_{\text{sec},i}^{H}(\ell)\,, \qquad (7)$$

where it should be noted that, unlike (6), the CUT snapshot is included in the SCM estimate of (7) because *a*) the range domain smearing makes it pointless to remove and *b*) the smearing also serves to diminish the response of a target of interest in the CUT. As above, diagonal loading may likewise be used with (7). Finally, the SCM estimates in (6) and (7) can also be combined as

$$\hat{\mathbf{R}}_{\mu}(\ell_{\text{CUT}})=\hat{\mathbf{R}}_{\text{prime}}(\ell_{\text{CUT}})+\hat{\mathbf{R}}_{\mu,\text{NP}}(\ell_{\text{CUT}})\,, \qquad (8)$$

again with the prospect of including diagonal loading.

III. Multi-Window Post-Doppler μ-STAP

As outlined in [4], practical implementation of STAP requires reduced dimension techniques due to real world limitations on sample support and computational cost. Following in the steps of [10], here we use forms of element-space multi-window post-Doppler STAP developed in [11,12] to implement reduced dimension μ-STAP.

Multi-window post-Doppler STAP applies different Doppler filters to the pulsed echoes received at the N antenna elements. Each antenna element has an identical bank of D filters for the mth Doppler bin. Let $\tilde{\mathbf{F}}_m$ be a $M\times D$ matrix comprised of D length-M filters for the mth Doppler bin. A $MN\times DN$ space-time transformation matrix is formed from this Doppler filter matrix as

$$\mathbf{T}_m=\tilde{\mathbf{F}}_m\otimes\mathbf{I}_N\,, \qquad (9)$$

where $\mathbf{I}_N$ is the $N\times N$ identity matrix corresponding to the N antenna elements. For the collection of space-time snapshots resulting from application of the $K+1$ range-domain filters in (2), the transformation of (9) is applied to produce the set of $DN\times 1$ transformed primary and secondary space-time snapshots for the mth Doppler bin as

$$\begin{aligned}\tilde{\mathbf{z}}_{\text{prime},m}(\ell)&=\mathbf{T}_m^{H}\mathbf{z}_{\text{prime}}(\ell)\\ \tilde{\mathbf{z}}_{\text{sec},1,m}(\ell)&=\mathbf{T}_m^{H}\mathbf{z}_{\text{sec},1}(\ell)\\ &\vdots\\ \tilde{\mathbf{z}}_{\text{sec},K,m}(\ell)&=\mathbf{T}_m^{H}\mathbf{z}_{\text{sec},K}(\ell)\end{aligned}\,. \qquad (10)$$

Similarly, this transformation matrix is applied to the space-time steering vector such that

$$\tilde{\mathbf{c}}_{\text{st},m}(\theta_{\text{prime}},\omega_{\text{D}})=\mathbf{T}_m^{H}\mathbf{c}_{\text{st}}(\theta_{\text{prime}},\omega_{\text{D}})\,. \qquad (11)$$

Incorporating (10) into (6)-(8) realizes the mth transformed SCMs where

$$\tilde{\mathbf{R}}_{\text{prime},m}(\ell_{\text{CUT}})=\mathbf{T}_m^{H}\hat{\mathbf{R}}_{\text{prime}}(\ell_{\text{CUT}})\mathbf{T}_m \qquad (12)$$

$$\tilde{\mathbf{R}}_{\mu,\text{NP},m}(\ell_{\text{CUT}})=\mathbf{T}_m^{H}\hat{\mathbf{R}}_{\mu,\text{NP}}(\ell_{\text{CUT}})\mathbf{T}_m \qquad (13)$$

$$\tilde{\mathbf{R}}_{\mu,m}(\ell_{\text{CUT}})=\mathbf{T}_m^{H}\hat{\mathbf{R}}_{\mu}(\ell_{\text{CUT}})\mathbf{T}_m\,. \qquad (14)$$

The mth transformed adaptive filter $\tilde{\mathbf{w}}_m(\ell_{\text{CUT}},\theta_{\text{prime}},\omega_{\text{D}})$ is then obtained by inserting (11) and the given SCM into (4) as

$$\tilde{\mathbf{w}}_m(\ell_{\text{CUT}},\theta_{\text{prime}},\omega_{\text{D}})=\left(\mathbf{T}_m^{H}\hat{\mathbf{R}}(\ell_{\text{CUT}})\mathbf{T}_m\right)^{-1}\mathbf{T}_m^{H}\mathbf{c}_{\text{st}}(\theta_{\text{prime}},\omega_{\text{D}}), \qquad (15)$$

where $\hat{\mathbf{R}}(\ell_{\text{CUT}})$ could be from (12), (13), or (14).

For the purpose of analysis, the mth transformed adaptive filter is best expressed by mapping it onto the full MN-dimensional space using the composite filter as [4]

$$\mathbf{w}_m(\ell_{\text{CUT}},\theta_{\text{prime}},\omega_{\text{D}})=\mathbf{T}_m\tilde{\mathbf{w}}_m(\ell_{\text{CUT}},\theta_{\text{prime}},\omega_{\text{D}}) \qquad (16)$$

via the transformation from (9). Thus

$$\mathbf{w}_m(\ell_{\text{CUT}},\theta_{\text{prime}},\omega_{\text{D}})=\mathbf{T}_m\left(\mathbf{T}_m^{H}\hat{\mathbf{R}}(\ell_{\text{CUT}})\mathbf{T}_m\right)^{-1}\mathbf{T}_m^{H}\mathbf{c}_{\text{st}}(\theta_{\text{prime}},\omega_{\text{D}}) \qquad (17)$$

is the full-dimension representation of the adaptive filter from (15) that shall be used for SINR analysis.

A. PRI-Staggered Post-Doppler

For this implementation, given M pulses in a CPI there will be $M'=M\ D+1$ sub-CPIs, for D the number of successive pulses in a sub-CPI. Let $\mathbf{U}=[\mathbf{u}_0\ \mathbf{u}_1\cdots\mathbf{u}_{M-1}]$ be an $M'\times M$ matrix constructed from the first M' rows of an $M\times M$ DFT matrix and $\mathbf{b}_{\text{PRI}}$ an $M'\times 1$ taper. Thus define the mth Doppler filter as [11]

$$\mathbf{f}_m=\mathbf{b}_{\text{PRI}}\odot\mathbf{u}_m^{*} \qquad (18)$$

for $m=0,1,\ldots,M-1$ and $(\bullet)^{*}$ complex conjugation. This filter is used to construct the mth Toeplitz Doppler filter matrix [11]

$$\tilde{\mathbf{F}}_m = \begin{bmatrix} \mathrm{f}_m(0) & 0 & \cdots & \cdots & 0 & 0 \\ \mathrm{f}_m(1) & \mathrm{f}_m(0) & \ddots & & \vdots & \vdots \\ \vdots & \mathrm{f}_m(1) & \ddots & \ddots & \vdots & \vdots \\ \mathrm{f}_m(M'-1) & \vdots & & \ddots & 0 & \vdots \\ 0 & \mathrm{f}_m(M'-1) & & & \mathrm{f}_m(0) & 0 \\ \vdots & 0 & \ddots & & \mathrm{f}_m(1) & \mathrm{f}_m(0) \\ \vdots & \vdots & \ddots & \ddots & \vdots & \mathrm{f}_m(1) \\ \vdots & \vdots & & \ddots & \mathrm{f}_m(M'-1) & \vdots \\ 0 & 0 & \cdots & \cdots & 0 & \mathrm{f}_m(M'-1) \end{bmatrix} \quad (19)$$

for the PRI-Staggered implementation.

B. Adjacent-Bin Post-Doppler

For this implementation let $\mathbf{U}$ be an $M \times M$ DFT matrix and $\mathbf{b}_{\mathrm{AB}}$ be an $M \times 1$ taper. The Doppler filter bank is defined as [12]

$$\mathbf{f}_m = \mathbf{b}_{\mathrm{AB}} \odot \mathbf{u}_m^* \quad (20)$$

for $m = 0, 1, \ldots, M-1$. The mth Doppler filter matrix comprises the surrounding Doppler filters from $m-P, \ldots, m+P$ for $P = (D-1)/2$, such that [12]

$$\tilde{\mathbf{F}}_m = \left[\begin{array}{ccccc} \mathbf{f}_{m-P} & \cdots & \mathbf{f}_m & \cdots & \mathbf{f}_{m+P} \end{array} \right]. \quad (21)$$

This Doppler filter matrix is designed to wrap around edges of the Doppler space.

IV. SINR Analysis

Using the SNR-normalized SINR metric from [5] within this reduced dimension framework, we compare standard STAP and μ-STAP to the optimal SINR as a function of sample support. Using the clairvoyant covariance matrix $\mathbf{R}_{\mathrm{opt}}$ and the adaptive filter formulation from (17), which is dependent on the choice of SCM from (12)-(14), the SINR for the reduced dimension implementation is [4]

$$\mathrm{SINR}(\quad) = \max_m \left\{ \frac{\left| \mathbf{w}_m^H \mathbf{c}_{\mathrm{st}} \right|^2}{\mathbf{w}_m^H \mathbf{R}_{\mathrm{opt}} \mathbf{w}_m} \right\}, \quad (22)$$

where the dependencies on ℓ_{CUT}, θ_{prime}, and ω_{D} have been suppressed. If we set $\hat{\mathbf{R}}(\ell_{\mathrm{CUT}}) = \mathbf{R}_{\mathrm{opt}}$ and $\mathbf{T}_m = \mathbf{I}_{NM}$, then (22) becomes the full-dimension optimum SINR denoted as

$$\mathrm{SINR}_{\mathrm{opt}}(\omega) = \mathbf{c}_{\mathrm{st}}^H \mathbf{R}_{\mathrm{opt}}^{-1} \mathbf{c}_{\mathrm{st}}. \quad (23)$$

We use the ratio of (22) to (23),

$$\frac{\mathrm{SINR}(\omega)}{\mathrm{SINR}_{\mathrm{opt}}(\omega)} = \max_m \left\{ \frac{\left| \mathbf{w}_m^H \mathbf{c}_{\mathrm{st}} \right|^2}{\mathbf{w}_m^H \mathbf{R}_{\mathrm{opt}} \mathbf{w}_m} \right\} \frac{1}{\mathbf{c}_{\mathrm{st}}^H \mathbf{R}_{\mathrm{opt}}^{-1} \mathbf{c}_{\mathrm{st}}}, \quad (24)$$

to evaluate the performance of STAP (using (12)) and μ-STAP (using (14)) for these reduced-dimension implementations as a function of sample support. For each clutter scenario, the mean performance is assessed across Doppler, excluding the clutter notch. In addition, SNR-normalized SINR Doppler is also examined for $2NM$ samples.

The analysis for partially adaptive μ-STAP follows that used in [2,3]. We considered a side-looking radar with $N = 11$ antenna elements in a uniform linear array (with $\lambda/2$ spacing), $M = 21$ pulses in the CPI, no crab angle, and β=1, where β is the number of half-interelement spacings traveled during one CPI. The clutter-to-noise ratio is 54 dB, where the noise is complex white Gaussian and the clutter is generated by dividing the range ring in azimuth into 241 equal-sized clutter patches, with each patch nominally being i.i.d. complex Gaussian (and further modified for non-homogeneous clutter). To account for angle-independent channel mismatch, a 30-dB Chebychev taper is applied to the spatial steering vector in (3) per

$$\hat{\mathrm{c}}_s(\theta_{\mathrm{prime}}) = \mathrm{t} \odot \mathrm{c}_s(\theta_{\mathrm{prime}}). \quad (25)$$

where $\mathbf{t}$ is a $N \times 1$ taper [14].

For dimension reduction, D = 5 and 10 pulses in a sub-CPI are examined. Per [10], a 20-dB Chebychev taper is used for PRI-Staggered while Adjacent-Bin uses a uniform taper. The number of range sample intervals used for SCM estimation is varied from 1 to $2NM$ = 462, noting that for μ-STAP this number is actually (K+1) to 2(K+1)NM due to the inclusion of training data from the K secondary filters. All SCM estimates are diagonally loaded with the noise power. For each scenario, 50 independent Monte Carlo trials are performed.

For all cases the emitted waveform is an optimized polyphase-coded FM (PCFM) waveform with time-bandwidth product BT = 100 [13]. The SISO mode (standard STAP via (12)), then applies the associated matched filter on receive. The SIMO mode (μ-STAP via (14)) additionally employs the K = 4 secondary pulse compression filters from (2). All of these filters correspond to different PCFM waveforms that are not transmitted and are related to the primary per Table I.

TABLE I. PRIMARY/SECONDARY PULSE COMPRESSION FILTERS FOR (2)

Filter	Characteristics
Primary	MF for optimized waveform with BT = 100 [13]
Secondary (k = 1)	Low cross-correlation with primary
Secondary (k = 2)	Time-reversed complex conjugate of primary
Secondary (k = 3)	Time-reversed complex conjugate of k = 1
Secondary (k = 4)	PCFM-implemented LFM [13]

TABLE II. RECEIVE PROCESSING CONFIGURATIONS

Filtering	Line style/color
STAP (K = 0), Full (M = 21)	solid blue
STAP(K = 0), Reduced (D = 10)	solid green
STAP(K = 0), Reduced (D = 5)	solid red
μ-STAP (K = 4), Full (M = 21)	dashed blue
μ-STAP (K = 4), Reduced (D = 10)	dashed green
μ-STAP (K = 4), Reduced (D = 5)	dashed red

Four clutter environments are used to assess performance of reduced dimension μ-STAP: 1) homogenous clutter, 2) non-homogeneous clutter, 3) homogeneous clutter with a large discrete in the CUT, and 4) large target in training data. Table II delineates the different receive processing configurations that are applied to the different clutter environments.

A. *Homogenous Clutter*

For Adjacent-Bin and PRI-Staggered, respectively, Figs. 1 and 2 show the mean SINR loss over Doppler (excluding the clutter notch) as a function of range sample intervals. In general, every version of μ-STAP outperforms its standard STAP counterpart in terms of convergence speed (significantly so) and SINR loss (at least by a small amount). Note that, for both reduced dimension implementations, as the dimensionality decreases from full dimension $M = 21$ (blue) to $D = 10$ (green) and again to $D = 5$ (red), the SINR loss at $2NM$ suffers about 1 dB loss relative to full STAP. Likewise, Figs. 3 and 4 depict SINR vs. Doppler for $2ND = 220$ (for D=10).

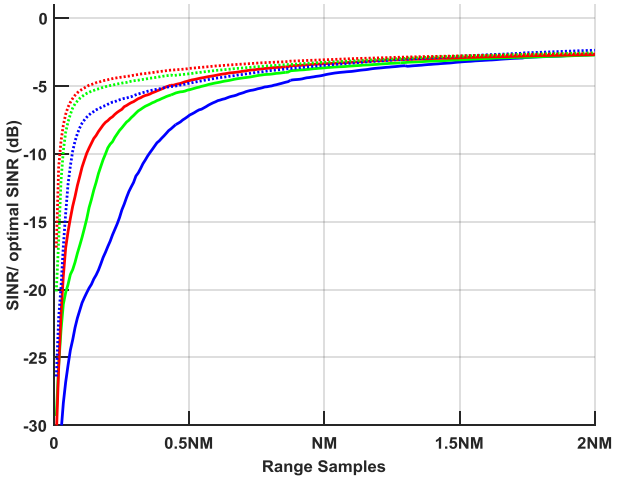

Fig. 1. Mean SINR/ SNR_{opt} for Adjacent-Bin in homogenous clutter

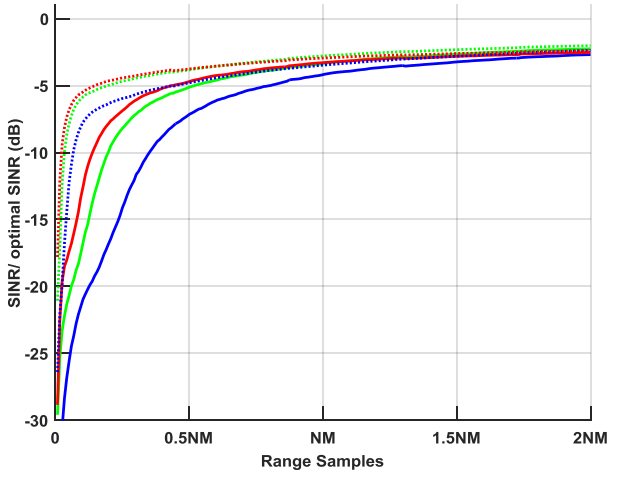

Fig. 2. Mean SINR/ SNR_{opt} for PRI-Staggered in homogenous clutter

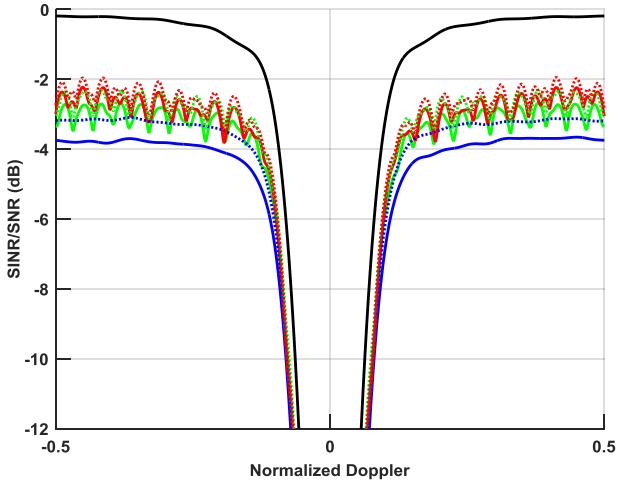

Fig. 3. SNR-normalized SINR for Adjacent-Bin in homogeneous clutter using $2ND$ range sample intervals

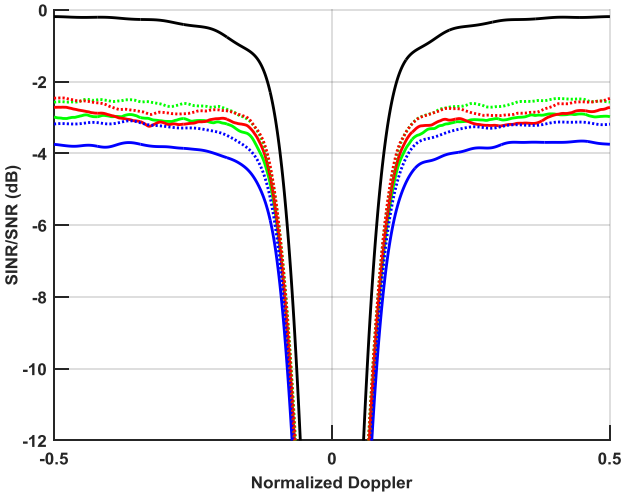

Fig. 4. SNR-normalized SINR for PRI-Staggered in homogeneous clutter using $2ND$ range sample intervals

B. *Non-homogenous Clutter*

Non-homogeneous clutter is modeled by randomly modulating the magnitude of each (already random) clutter patch in range/angle, based on a uniform distribution drawn from [0, 30] dB. Further, internal clutter motion is modeled as a uniform distribution on ±2% of the normalized Doppler.

Figures 5 and 6 illustrate the Adjacent-Bin and PRI-Staggered results, respectively, for this case. Aside from the expected slower convergence due to non-homogeneous clutter, it is observed that the performance relationships between the various cases is more or less unchanged.

Figures 7 and 8 depict the Adjacent-Bin and PRI-Staggered SNR-normalized SINR results at $2ND$ (for D=10) range sample intervals, respectively, as a function of Doppler. It is observed that, as expected, the clutter notch is wider and performance across all cases degraded to some degree (though the reduced-dimension μ-STAP results experience the least degradation).

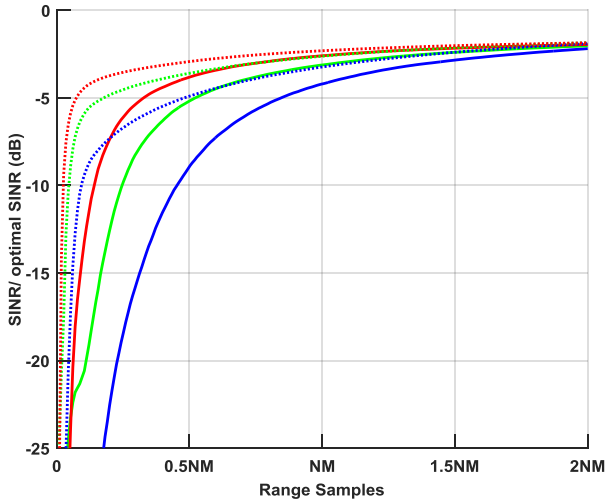

Fig. 5. Mean SINR/ SNR_{opt} for Adjacent-Bin in non-homogenous clutter

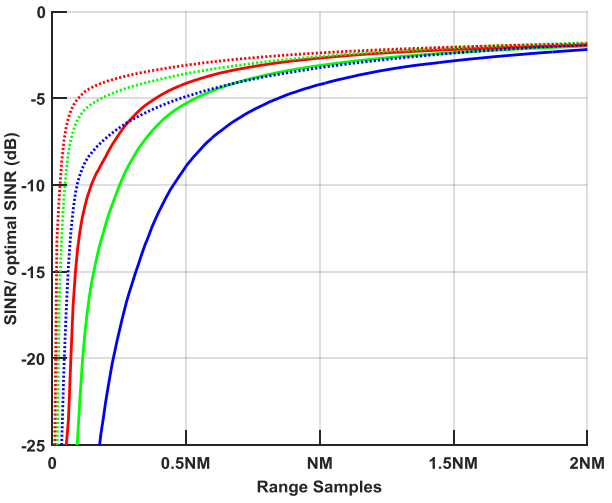

Fig. 6. Mean SINR/ SNR_{opt} for PRI-Staggered in non-homogenous clutter

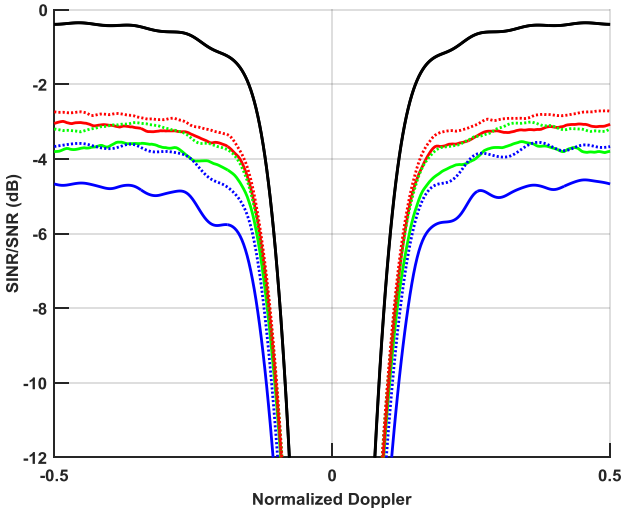

Fig. 7. SNR-normalized SINR for Adjacent-Bin in non-homogeneous clutter using 2*ND* range sample intervals

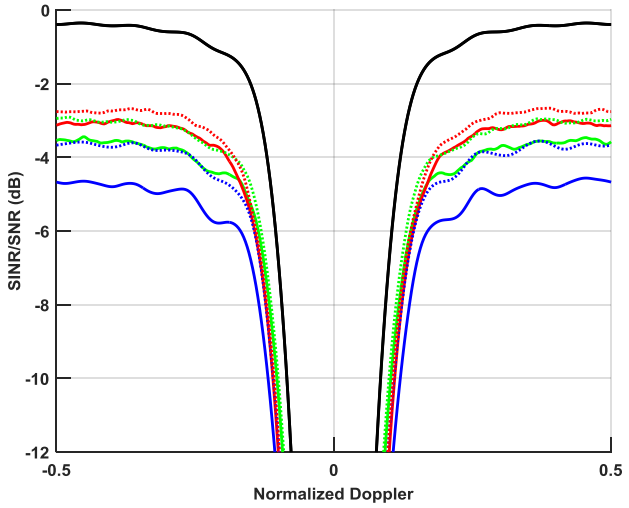

Fig. 8. SNR-normalized SINR for Adjacent-Bin in non-homogeneous clutter using 2*ND* range sample intervals

C. Clutter Discrete in CUT

In this case a large clutter discrete (40 dB > average clutter power) is present in the CUT, with the clutter otherwise being homogeneous. The convergence results are generally similar to the previous results (and thus not shown), but it is observed across Doppler in Figs. 9 and 10 (for 2*ND* range sample intervals with D=10) that the faster convergence of the reduced dimension implementations yield less SINR loss than full-dimension. Here the reduced dimension μ-STAP results only marginally surpass that of reduced dimension STAP.

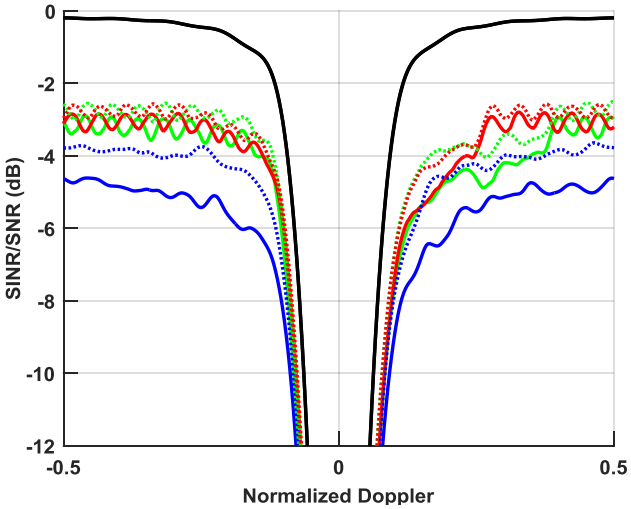

Fig. 9. SNR-normalized SINR for Adjacent-Bin with clutter discrete using 2*ND* range sample intervals

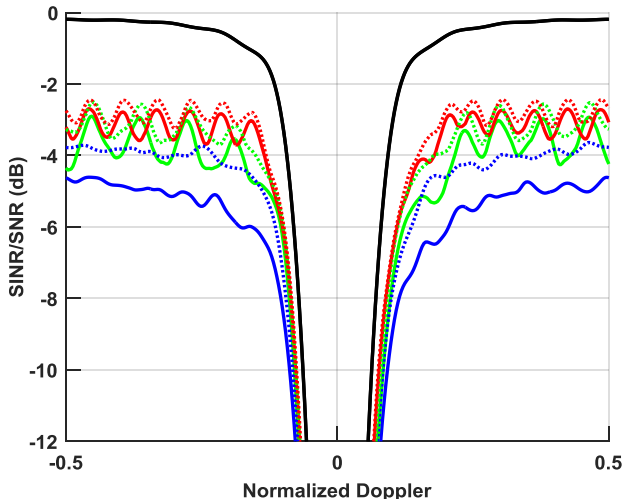

Fig. 10. SNR-normalized SINR for PRI-Staggered with clutter discrete using 2*ND* range sample intervals

D. Large Target in Training Data

In this scenario, a large target (30 SNR) is placed in the first training data sample with a normalized Doppler of 0.5. The μ-STAP convergence advantage is again similar to earlier results. However, the additional benefit observed here is the shallower null produced by the large training data target when using μ-STAP with the $D = 5$ (dashed red) implementations.

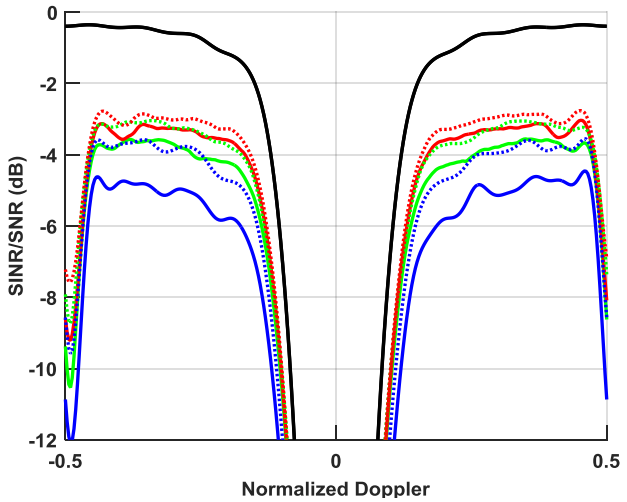

Fig. 11. SNR-normalized SINR for Adjacent-Bin with target in training data using 2*ND* range sample intervals

V. CONCLUSIONS

It was previously shown that μ-STAP provides some enhanced robustness to non-stationary interference due to the smearing effect it produces in range prior to SCM estimation. Here it was shown that μ-STAP is likewise amenable to reduced-dimension implementations that are more practical than full-dimension STAP due to computational cost and sample support limitations. Further, within the reduced-dimension context, it was observed that μ-STAP provides an SINR advantage over standard STAP, particularly at low sample support. Note that for 5*NM* sample intervals (not shown) full-dimension performance does surpass that of reduced dimension as expected.

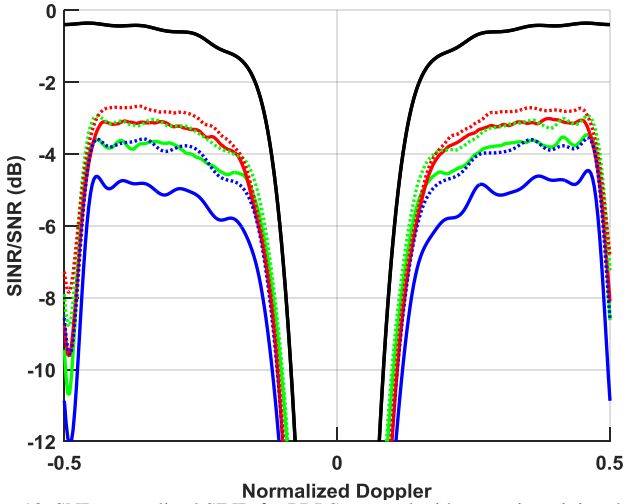

Fig. 12. SNR-normalized SINR for PRI-Staggered with target in training data using 2*ND* range sample intervals

REFERENCES

[1] S.D. Blunt. J. Jakabosky, J. Metcalf, J. Stiles, B. Himed, "Multi-waveform STAP," *IEEE Radar Conf.,* Ottawa, Canada, Apr.-May 2013.

[2] S.D. Blunt, J. Metcalf, J. Jakabosky, and B. Himed, "SINR analysis of multi-waveform STAP," *Intl. Radar Conf.,* Lille, France, Oct 2014.

[3] S.D. Blunt, J. Metcalf, J. Jakabosky, J. Stiles, B. Himed, "Multi-waveform space-time adaptive processing," to appear in *IEEE Trans. AES.*

[4] J. Ward, "Space-time adaptive processing for airborne radar," *Lincoln Lab Tech. Report,* TR-1015, Dec. 1994.

[5] W.L. Melvin, "A STAP overview," *IEEE AES Systems Mag.*, vol. 19, no.1, pp.19-35, Jan. 2004.

[6] K. Gerlach, "Outlier resistance adaptive matched filtering," *IEEE Trans. AES*, vol. 38, no. 3, pp. 885-901, July 2002.

[7] W.L. Melvin, "Space-time adaptive radar performance in heterogenous clutter," *IEEE Trans. AES*, vol. 36, no. 2, pp. 621-633, Apr. 2000.

[8] M.Rangaswamy, P.Chan, J.H. Michels, and B. Himed, "A comparison of two non-homogeneity detection methods for space-time adaptive processing," *IEEE SAM Workshop,* Aug. 2002.

[9] K. Gerlach, S.D. Blunt, and M.L. Picciolo, "Robust adaptive matched filtering using the FRACTA algorithm," *IEEE Trans. AES,* pp. 929-945, July 2004.

[10] A.K. Shackelford, K. Gerlach, S.D. Blunt, "Partially adaptive STAP using the FRACTA algorithm," *IEEE Trans. AES*, vol. 45, no. 1, pp. 58-69, Jan. 2009.

[11] J. Ward and A.O. Steinhardt, "Multiwindow post-Doppler space-time adaptive processing," *IEEE Statistical Signal & Array Processing Workshop*, Quebec, Canada, June 1994.

[12] R.C. DiPietro, "Extended factored space-time processing for airborne radar," *Asilomar Conf.*, Pacific Grove, CA, Oct. 1992.

[13] S.D. Blunt, J.Jakabosky, M. Cook, J. Stiles, S. Seguin, and E.L. Mokole, "Polyphase-coded FM (PCFM) radar waveforms, part II: optimization," vol. 50, no. 3, pp. 2230-2241, July 2014.

[14] J.R. Guerci, "Other important factors affecting STAP performance" *Space-Time Adaptive Processing for Radar,* Artech House, 2003.